Low frequency dynamics of the nitrogenase MoFe protein via femtosecond pump probe spectroscopy — Observation of a candidate promoting vibration

Margherita Maiuri [a], Ines Delfino [b], Giulio Cerullo [a], Cristian Manzoni [a], Vladimir Pelmenschikov [c], Yisong Guo [d], Hongxin Wang [e], Leland B. Gee [e], Christie H. Dapper [f], William E. Newton [f], Stephen P. Cramer [e,g,*]

[a] IFN-CNR, Dipartimento di Fisica, Politecnico di Milano, Piazza Leonardo da Vinci 32, I-20133 Milano, Italy
[b] Dipartimento di Scienze Ecologiche e Biologiche, Università della Tuscia, Largo dell'Università, I-01100 Viterbo, Italy
[c] Institut für Chemie, Technische Universität Berlin, Strasse des 17 Juni 135, 10623 Berlin, Germany
[d] Department of Chemistry, Carnegie Mellon University, Pittsburgh, PA 15213, United States
[e] Department of Chemistry, University of California, Davis, CA 95616, United States
[f] Department of Biochemistry, Virginia Polytechnic Institute & State University, Blacksburg, VA 24061, United States
[g] Physical Biosciences Division, Lawrence Berkeley National Laboratory, Berkeley, CA 94720, United States

ARTICLE INFO

ABSTRACT

We have used femtosecond pump-probe spectroscopy (FPPS) to study the FeMo-cofactor within the nitrogenase (N_2ase) MoFe protein from *Azotobacter vinelandii*. A sub-20-fs visible laser pulse was used to pump the sample to an excited electronic state, and a second sub-10-fs pulse was used to probe changes in transmission as a function of probe wavelength and delay time. The excited protein relaxes to the ground state with a ~1.2 ps time constant. With the short laser pulse we coherently excited the vibrational modes associated with the FeMo-cofactor active site, which are then observed in the time domain. Superimposed on the relaxation dynamics, we distinguished a variety of oscillation frequencies with the strongest band peaks at ~84, 116, 189, and 226 cm^{-1}. Comparison with data from nuclear resonance vibrational spectroscopy (NRVS) shows that the latter pair of signals comes predominantly from the FeMo-cofactor. The frequencies obtained from the FPPS experiment were interpreted with normal mode calculations using both an empirical force field (EFF) and density functional theory (DFT). The FPPS data were also compared with the first reported resonance Raman (RR) spectrum of the N_2ase MoFe protein. This approach allows us to outline and assign vibrational modes having relevance to the catalytic activity of N_2ase. In particular, the 226 cm^{-1} band is assigned as a potential 'promoting vibration' in the H-atom transfer (or proton-coupled electron transfer) processes that are an essential feature of N_2ase catalysis. The results demonstrate that high-quality room-temperature solution data can be obtained on the MoFe protein by the FPPS technique and that these data provide added insight to the motions and possible operation of this protein and its catalytic prosthetic group.

© 2015 Elsevier Inc. All rights reserved.

1. Introduction

Reduction of N_2 to NH_3 is the most difficult reaction in the nitrogen cycle [1]. Biological nitrogen fixation (BNF) is ultimately responsible for about half of the reductive part of the nitrogen cycle and half of the food produced globally each year [4,5]. The other half of global nitrogen fixation is accomplished in the fossil-fuel dependent Haber–Bosch process, which is estimated to contribute to about 2% of the world's CO_2 emissions [4,5]. The enzyme responsible for BNF is known as nitrogenase (N_2ase) [6–8]. The most studied versions of N_2ase involve a ~250 kDa $\alpha_2\beta_2$ MoFe protein which is reduced by a ~60 kDa Fe protein during catalysis [9,10]. Other less efficient N_2-reducing enzymes are known that have a VFe- or FeFe-protein substituting for the MoFe protein [11,12].

In the *Azotobacter vinelandii* (*Av*) Mo-dependent N_2ase, catalysis takes place at an active site [Mo–7Fe–9S-C_i](*R*-homocitrate) 'FeMo-cofactor' [15] (see Fig. 1), with the interstitial light atom [16] recently identified as carbide (Ci) [2,13,14]. Over the past decade, there has been substantial progress in understanding the role of this cofactor in N_2ase catalysis [7, 17,18]. The Fe2–Fe3–Fe6–Fe7 face has been identified as the most likely site for substrate binding with the neighboring α-70Val side chain modulating substrate access to this face [19]. Known catalytic capabilities of N_2ase have been recently expanded to include CO and even CO_2 reduction with production of C1 to C4 hydrocarbons [20–23].

Using EPR and ENDOR spectroscopies [18], bound acetylenic [24], hydridic [25], or nitrogenous [26–29] species have been identified. Using stopped-flow IR spectroscopy, variations in the rate and type of CO binding have been observed for variant MoFe proteins with amino-
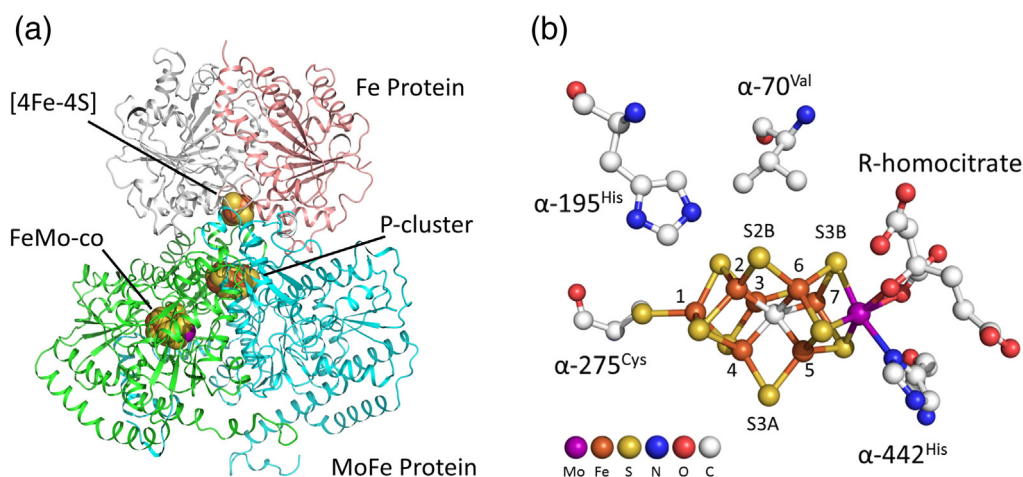
Fig. 1. (a) Structure of half of the N$_2$ase MoFe protein α$_2$β$_2$ dimer, complexed with the Fe protein (PDB ID: 1N2C) [9]. (b) Local structure around the FeMo-cofactor, highlighting the Fe2–Fe3–Fe6–Fe7 face (PDB ID: 3U7Q) [13,14].

acid substitutions at the α-70Val side chain position [30]. IR-monitored photolysis of frozen CO-inhibited N$_2$ase solutions has revealed evidence for both terminal and 'formyl-like' CO ligands, in some cases, bound to EPR-silent FeMo-cofactor forms [31,32]. The combination of NRVS and EXAFS, together with DFT calculations, has offered evidence for significant structural changes upon binding of CO [33] or nitrogenous ligands [34].

Despite this progress, our knowledge of the N$_2$ase mechanism can be compared to the 'dark matter' problem facing high-energy physicists. Even one of the simplest questions – where and how does N$_2$ initially bind at the active site – remains debated. Many of the N$_2$ase intermediates may be diamagnetic and hence 'dark' to EPR. Other intermediates are likely missed by IR methods because key bands are obscured by protein features or diminished by selection rules. New approaches to probing this enzyme are clearly needed. Since many of the methods currently in use (EPR, ENDOR, EXAFS, Mössbauer, and NRVS) are usually conducted under cryogenic conditions, new room temperature solution techniques would be especially valuable for probing the catalytic mechanism.

In this paper, we report the use of femtosecond pump-probe spectroscopy (FPPS) to observe, in the time domain, vibrational modes of the FeMo-cofactor in the MoFe protein that have been impulsively excited by an ultrashort laser pulse. The FPPS technique (alternatively called 'impulsive coherent vibrational spectroscopy') has successfully been applied for observing vibrational modes in other metalloproteins such as blue copper proteins [35–39] and heme proteins [40–42], and it was previously used by some of the authors to characterize the isolated N$_2$ase cofactor, 'FeMo-co' [43] (the cluster that can be extracted into NMF solvent upon denaturing the MoFe protein). Here, we compare the FPPS results with the data from NRVS and Resonance Raman (RR) spectroscopies. We use empirical force field (EFF) and density functional theory (DFT) calculations to interpret the spectra. This enables us to assign the observed vibrational modes, and discuss their relevance to N$_2$ase activity. In particular, the 226 cm^{-1} mode is thought to be a potential 'promoting vibration' in the H-atom transfer (or proton-coupled electron transfer) processes. Taken together, our results demonstrate that the FPPS technique can be used to observe the ground state vibrational dynamics on the intact protein in solution at reasonable concentrations, thus offering a potential route to characterization of CO-inhibited species as well as reactive N$_2$-fixing intermediates.

2. Methods

2.1. MoFe protein preparation and purification

The *Av* wild-type strain was grown in the absence of a fixed-nitrogen source in a 24-L fermentor at 30 °C in a modified, liquid Burk medium [44] as described previously [45]. All manipulations of the N$_2$ase component proteins were performed anaerobically using either a Schlenk line or an anaerobic glove box operating at less than 1 ppm O$_2$. The N$_2$ase component proteins were separated by anaerobic Q-Sepharose anion-exchange column chromatography using a linear NaCl concentration gradient. The MoFe protein was further purified by Sephacryl S-200 gel filtration and phenyl-Sepharose hydrophobic-interaction chromatography [45]. The purified MoFe protein solution was concentrated using an Amicon micro-filtration pressure concentrator before buffer exchange to 25 mM HEPES (pH 7.4), 300 mM NaCl, 10 mM MgCl$_2$ and 2 mM Na$_2$S$_2$O$_4$. The purified wild-type MoFe protein had a specific activity of 2500 nmol H$_2$ (min·mg protein)$^{-1}$ at 30 °C when assayed in the presence of an optimal amount of the purified Fe protein as described previously [46]. Protein concentrations were determined by the Lowry method.

2.2. Femtosecond experiments

The experimental setup used for the FPPS experiment has been described in detail elsewhere [47]. Briefly, a 150-fs pulse (780-nm, 500-μJ at 1-kHz repetition rate), generated by a regeneratively-amplified mode-locked Ti:sapphire laser, drives two synchronized visible non-collinear optical parametric amplifiers (NOPAs). The first NOPA (NOPA1) generates pulses at 940 nm, which are frequency-doubled to obtain the pump pulses centered at 470 nm, in order to selectively excite the N$_2$ase MoFe protein in resonance with its ground-state blue absorption. The second NOPA (NOPA2) generates broadband (500–700 nm) visible probe pulses. Both NOPAs are compressed to nearly transform-limited duration by either a prism pair (for NOPA1) or multiple bounces on chirped mirrors (for NOPA2), retrieving 15-fs pulses for NOPA1 and nearly 7-fs pulses for NOPA2. The pump and probe pulses are superimposed on the sample in a slightly non-collinear geometry and their delay is controlled by a motorized translation stage. The pump pulse is modulated at 500 Hz by a chopper wheel. After the sample, the probe beam is focused onto the entrance slit of a spectrometer equipped with a linear photodiode array with fast electronics allowing a full 1-kHz read-out rate [47,48]. By recording pump-on and pump-off probe spectra, we calculate the differential transmission (ΔT/T) signal as a function of probe wavelength λ and pump-probe delay τ as: ΔT / T(λ,τ) = (T$_{on}$(λ,τ) − T$_{off}$ (λ)) / T$_{off}$ (λ). Pump-probe experiments were performed on the MoFe protein sample in a 1-mm pathlength cuvette sealed to prevent exposure to atmospheric oxygen.

2.3. Raman measurements

RR spectra were recorded in a backscattering geometry from a solution of the MoFe protein in either H_2O or D_2O. Each measurement sample (~5 µl) was first loaded into a Hamilton gas-tight syringe inside a nitrogen atmosphere glovebox (O_2 level < 1 ppm). The syringe was moved out of the glovebox and the sample solution was quickly ejected onto a cooled copper disk, which was then immediately immersed in liquid nitrogen (LN_2). The sample was exposed to air at room temperature for less than 10 s. The sample (with copper disk) was then mounted onto the sample rod under LN_2 and the rod then relocated into a LN_2 cryostat (Oxford Optostat) maintained at 77 K. The excitation source was a cw Ar/Kr ion laser (Coherent, Innova-70-200) operated at 488 nm (power = 80 mW) or a cw HeCd laser (Kimmon, IK5652R-G) operated at 442 nm (power = 40 mW). The spectra shown in Fig. 4 were measured at 488 nm. No spectral changes were observed as measurement time increased. Nevertheless samples were changed every 16 h (one day's measurement). The spectra were recorded with a Spex model 1877 triple Raman spectrometer, using a LN_2 cooled Spectrum One 594 CCD detector. The N_2ase-H_2O (and N_2ase-D_2O) spectra correspond to data from 74 (132 for N_2ase-D_2O) hours of measurement. The spectra were calibrated using peaks at 218 and 314 cm^{-1} in a room temperature CCl_4 sample. The spectral resolution was 6–8 cm^{-1}.

2.4. EFF normal mode calculations

The empirical normal mode calculations used a Urey–Bradley force field [49] and a modification of the program 'Vibratz' [50,51] to simulate a vibrational stick spectra based on force constants for an internal coordinate system. Simulated spectra were generated by convolving the calculated stick spectra with an 8 cm^{-1} Gaussian. The force field is then optimized to match the spectrum using least squares fitting. The coordinates of the [Mo–7Fe–9S-C_i] cofactor core, together with atoms from the first coordination sphere of the cofactor core (including two oxygen atoms from *R*-homocitrate and one nitrogen atom from α-442His coordinated with Mo, one sulfur atom and the adjacent β-carbon from α-275Cys), were extracted from the 1.16 Å 1M1N PDB file [3,17]. This structure was further symmetrized to give a [$O_3MoFe_7C_iS_9(SC)$] structure with C_{3v} symmetry. All empirical normal mode calculations were performed based on this symmetrized structure.

2.5. DFT calculations

All the DFT calculations were performed using the PBE [52] functional and the LACV3P** basis set as implemented in *JAGUAR 7.9* [53] software. For the first- and second-row elements, LACV3P** implies a 6-311G** triple-zeta basis set including a polarization function. For Fe and Mo atoms, LACV3P** uses the Los Alamos effective core potential (ECP), and the valence part is essentially of triple-zeta quality. The geometries, optimized at the PBE/LACV3P** level using *GAUSSIAN 03* [54] software, were used for the analytic Hessian calculations, resulting in the DFT Raman intensities and other vibrational properties discussed in the text. We found the present and essentially equivalent setups to perform well for the vibrational dynamics of several iron–sulfur systems [32,33,55–58]. The analysis of the computed normal modes was done using an in-house *Q-SPECTOR* Python tool to model the Raman spectra. A 6 cm^{-1} (FWHM) Lorentzian broadening of the calculated mode intensities was used.

2.5.1. Structural modeling

Initial coordinates for the [Mo–7Fe–9S-C_i] cofactor core and its immediate covalent ligands were extracted from the 1.16 Å 1M1N PDB file [14,16] as outlined above, but with α-275Cys simplified to methylthiolate, α-442His to imidazole, and R-homocitrate to glycolate ($^-OCH_2$–COO^-).

2.5.2. Metal sites oxidation level and spin coupling

The present modeling assumes [$Mo^{4+}3Fe^{3+}4Fe^{2+}$] formal oxidation levels for the transition metal ions comprising the FeMo-cofactor in the $S = 3/2$ resting state, as proposed earlier [59]. A set of seven Fe-site local spin vectors that satisfy the total FeMo-cofactor spin is not unique. Following the broken symmetry (BS) concept [60], we used the so-called BS7 spin-collinear coupling [61] for the Fe sites. The initial BS electronic structures were constructed using an option to assign a number of unpaired α/β electrons and formal charges to the Fe atomic fragments, as implemented in *JAGUAR 7.9*. The resulting self-consistent field (SCF) solutions bear a mixed-valence Fe^{3+}/Fe^{2+} character, however retaining the BS7 spin densities pattern.

3. Results

3.1. Femtosecond pump-probe spectroscopy

Fig. 2a shows both the absorption spectrum for the N_2ase MoFe protein and the spectra of the pump and probe pulses used. The absorption spectrum of the fully active MoFe protein is relatively featureless but, on oxidation, a diagnostically significant shoulder appears at ~435 nm [62]. Control experiments performed after the laser irradiation showed no change in the spectrum (see dashed line in Fig. 2a), which confirms the preservation of sample integrity throughout the femtosecond experiments. Fig. 2b shows a representative two-dimensional (2D) map of ΔT/T as a function of probe wavelength and pump-probe delay for the MoFe protein following the excitation by a ~18 fs pump pulse centered at 470 nm. Around zero pump-probe delay at all wavelengths, we observe a strong derivative-like response that lasts for ~100 fs. This signal arises from pump-probe cross-phase modulation induced by the non-resonant absorption of the buffer solution, as commonly observed in transient absorption measurements of protein solutions [63]. This artifact prevents the observation of very fast processes occurring in the first ~100 fs. After the buffer response has ceased, a ΔT / T > 0 signal is observed in the region between 500 and 630 nm. This signal is assigned to the superposition of photobleaching of the ground state and stimulated emission from the photoexcited state.

It is modulated by a complex oscillatory pattern that is evident throughout the analyzed time delay and probe wavelength range, and is assigned to vibrational coherence, created by the very short pump pulse in the excited and ground states multi-dimensional potential energy surfaces (PES) [64].

The ΔT/T signal decays on the picosecond timescale, indicating fast recovery of the ground-state population, with however some residual signal persisting beyond 2 ps. For all traces, a good description of the ΔT/T dynamics is given by a single exponential decay plus a constant offset: $y(t) = A \exp(-t/\tau) + y_0$. For probe wavelengths in the range of the broad positive band, a fit to this model gives a time constant $\tau = 1.16 \pm 0.08$ ps with an offset of about 20% of the initial signal (Fig. 2c). Similar results are obtained at other probe wavelengths.

The observed time constants for electronic relaxation are longer than those seen in other Fe–S and Cu–S protein systems. Blue Cu proteins have been reported to relax with time constants from 250 fs up to 700 fs [39], and lifetimes of ~250 and 200 fs have been observed for rubredoxin [65] and the isolated FeMo-co [43], respectively. This indicates that a weaker non-radiative coupling exists between the ground and the excited states in this system compared to other Fe–S and Cu–S protein systems. This relative isolation of the FeMo-cofactor seems reasonable, given that only 2 out of its 40 metal-ligand bonds involve amino acid side-chains. The constant offset, that appears stationary on the time scale of the measurements, could be evidence of a fraction of the population becoming trapped on an excited state surface and preventing the reestablishment of the equilibrium on the few picosecond time scale of the pump-probe experiments. In order to analyze
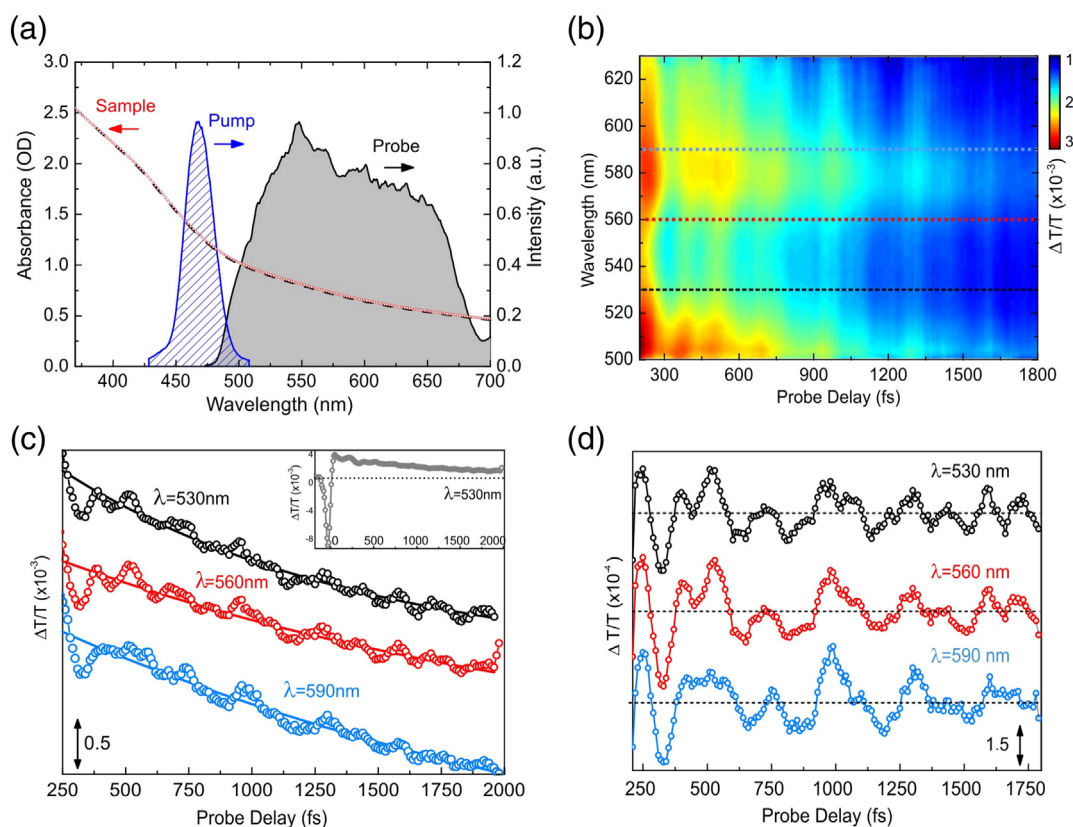
Fig. 2. (a) Absorption spectrum of the N₂ase MoFe protein before (red dotted line) and after (black dashed) measurement compared with pump spectrum at 470 nm (blue dashed), and broad probe spectrum (gray shadow). (b) 2D $\Delta T/T$ map of the N₂ase MoFe protein obtained after pumping with the 470 nm pulse. (c) $\Delta T/T$ traces measured (circles) and corresponding fits (solid lines) at probe wavelength of 530, 560 and 590 nm (black, red and light blue respectively dashed in b); the inset shows the whole dynamic, including the artifact at zero delay, for the 530 nm probe wavelength. (d) Oscillatory signals obtained after subtracting the slowly varying component from the $\Delta T/T$ traces at 530, 560 and 590 nm shown in c.

the oscillatory component superimposed on the $\Delta T/T$ signal, the slowly varying exponential decay was subtracted from the experimental data to produce the residuals, shown in Fig. 2c for the 530, 560 and 590 nm probe wavelengths, which clearly exhibit oscillations around the zero level. Although the general patterns are the same, differences among the shown residuals are observed, illustrating the dependence of the vibrational activity on the probe wavelength being used. The complex oscillatory patterns of the residuals are more easily visualized for all the probe wavelengths by means of Fourier Transform (FT) analysis. The results of this procedure are illustrated in Fig. 3, which displays a 2D map of the FT of the residuals (Fig. 3a), along with FT intensity spectra for probe wavelengths of 530, 560, and 590 nm (Fig. 3b). At most probe wavelengths from 520 to 620 nm, there are features in the 80–250 cm⁻¹ range. In particular for $\lambda = 530$ nm, strong peaks in the regions around 84, 116, 189, and 226 cm⁻¹ are observed. The absolute peak positions and the relative intensities of these bands also change across the probe spectrum. Weaker but reproducible features are also seen at around 250 and 276 cm⁻¹ and even out to 400 cm⁻¹ (see Fig. 4). Since the only chromophores absorbing in the visible presumably correspond to particular normal modes of the FeMo-cofactor and/or the P-cluster.

Some of the features have been seen before in FPPS experiments on isolated FeMo-co [43], but the improved statistics for the current data allow many additional bands to be confidently assigned. To better assign the observed frequencies, and also to show the strengths and limitations of the FPPS approach, we compare in Fig. 4 the time-domain data with both recent data from the NRVS spectrum for the FeMo-cofactor within the MoFe protein [33] and also with preliminary RR experimental results, here reported for the first time. The RR spectrum calculated from our DFT model is also shown in Fig. 4. The spectra display

similarities and peculiarities, which will be discussed in detail in the next section.

3.2. Normal mode calculations

As we will discuss in Section 4, we believe that the ~226 cm⁻¹ normal mode plays a significant role in the catalytic activity of the N₂ase enzyme. In Fig. 5, we illustrate the atomic motions for this mode, as predicted by two different computational methods. The EFF calculation was done for an idealized version of the FeMo-cofactor with C_{3v} symmetry, in order to minimize the number of adjustable parameters. In contrast, the DFT calculation started with the observed crystal structure. Despite these differences in structural modeling and computational methods (as detailed in the methods section), both EFF and DFT arrive at a similar description of the 226 cm⁻¹ mode; it is an approximately symmetric stretch of the FeMo-cofactor bridging sulfides.

3.3. Molecular dynamics

In Fig. 5, we also illustrate the distribution of the S2B–H(α-195His) distances (cf. Fig. 1b), derived from a molecular dynamics (MD) calculation using our FeMo-cofactor EFF calculation together with a typical protein force field. The force field development and its employment are detailed in our previous work [66]. We find that such a calculation predicts occasional closest approaches of 2.05 Å or less. As discussed below, at such distances it is feasible for a proton to tunnel between the histidine nitrogen and the bridging sulfide.
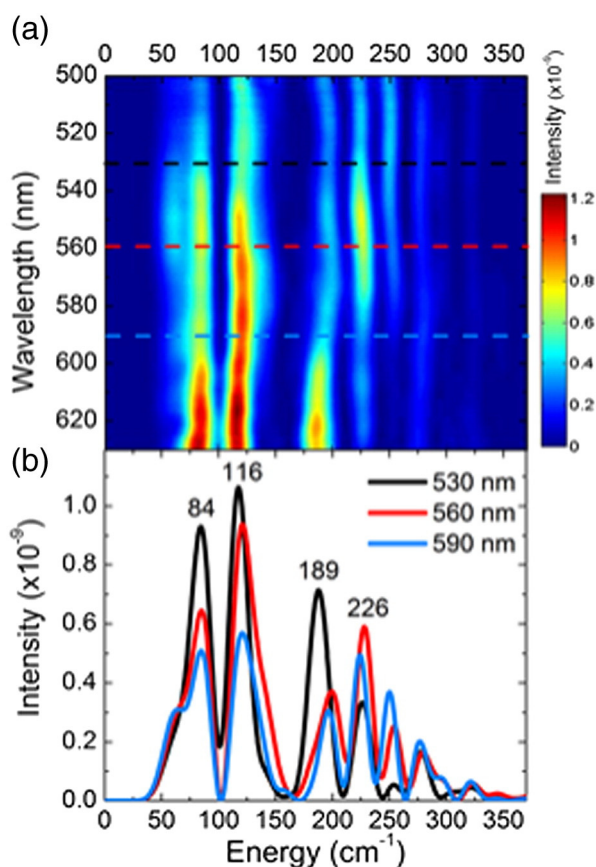
Fig. 3. (a) 2D FT of the ΔT/T map for the N₂ase MoFe protein as a function of probe wavelength (pump at 470 nm) after subtracting the slowly decaying signal. (b) Corresponding FT intensity spectra, for probe wavelengths at 530 (− − −); 560 (——), and 590 nm (——).

Fig. 4. Spectral comparisons for the N₂ase MoFe protein. (a) FPPS spectra of MoFe protein for probe wavelength at 530 nm; (b) NRVS data for the MoFe protein [33] and isolated FeMo-cofactor; (c) RR spectra (excited at 488 nm) for N2ase in H₂O or D₂O; (d) predicted Raman spectrum for FeMo-cofactor from DFT calculations.

4. Discussion

4.1. FPPS–NRVS–RR comparisons

This paper reports on the time-domain observation of low-frequency vibrational dynamics of nitrogenase MoFe protein by the FPPS technique. Although the production of coherent vibrational states by femtosecond pulses has been known for some time [67], the mechanism by which this technique reveals ground and excited state vibrational spectra is not always clear. It is well known that pump-probe spectroscopy involves a three-field interaction with the sample: two of these with the pump, creating a population, and one with the probe, which then interrogates it. For short pump pulses, two fields in the pump pulse can excite, in phase, several vibrational eigenstates of the excited state, creating a vibrational wave packet oscillating on the excited-state PES, leaving and returning to the Frank–Condon region (we refer to the work of Champion and coworkers for a slightly different description [68]). Another possibility is that the first field induces a polarization wave packet on the excited-state PES, which then propagates during the pump pulse so that the second interaction with the pump field brings the wave packet back down to the ground state, displaced from the equilibrium position. In this way, ground state oscillations are generated by a mechanism known as resonant impulsive stimulated Raman scattering [69]. A third mechanism is reaction-driven vibrational excitation, in which photolysis of a ligand such as CO or methionine delivers a momentum pulse to the remaining chromophore system [41,70,71]. In our case, since there is no photolysis, this third mechanism can be excluded. On the other hand, the assignment of the observed coherence to the ground or excited state vibrational activity and to specific modes is critical.
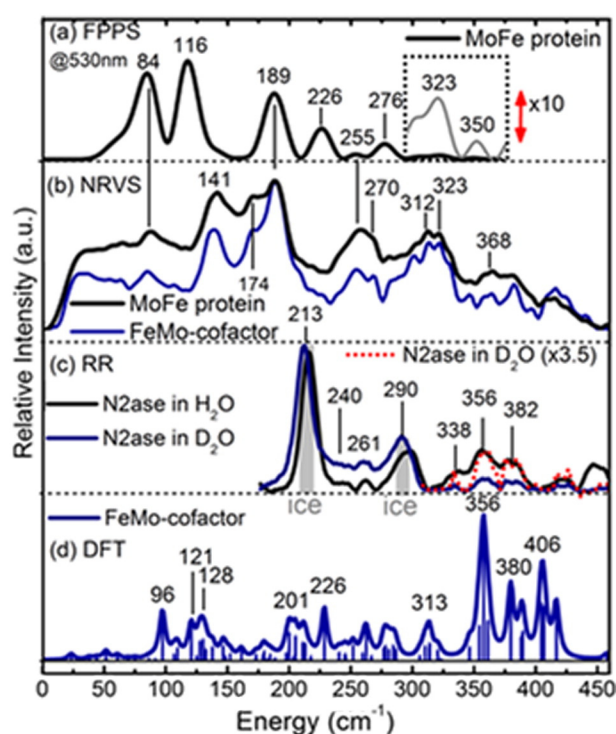
In comparing FPPS results with NRVS (and later with RR spectra) we note the limitation seen by Champion and coworkers for the 'accurate resolution of frequencies when many modes are active' [72], which is certainly the case with the large FeMo-cofactor. In the case of met-myoglobin, some FPPS frequencies deviated by as much as 10 cm⁻¹ from the corresponding RR values [72], although with improved statistics and a wider time domain this has improved to ±5 cm⁻¹ [41].

The lowest frequency FPPS major peak observed at ~84 cm⁻¹ corresponds nicely to a feature at the same location in the NRVS of both wild-type N₂ase MoFe protein and extracted FeMo-co. At slightly higher frequencies, there is an FPPS feature at 116 cm⁻¹. This region has intensity but no resolved peaks in the FeMo-cofactor NRVS, and so we cannot rule out assigning some or all of this intensity to the P-cluster. A much clearer correspondence between FPPS and NRVS occurs with the next FPPS feature at ~189 cm⁻¹ (monitored at 530 nm), which aligns with the NRVS peak at essentially the same position. Previous normal mode calculations suggested that there is a cluster of modes in this region [43,46]. The peak position moves to 199 or 196 cm⁻¹ when monitored at 560 or 590 nm, consistent with additional modes in this region. Here, the ability to distinguish at least 2 distinct bands by changing probe wavelengths demonstrates a real advantage of the FPPS technique. In contrast, these features are unresolved in the NRVS, where the current resolution is usually on the order of 8–10 cm⁻¹.

Another consistent FPPS feature is found at 220–226 cm⁻¹. The ~220 cm⁻¹ feature has been seen before in FPPS experiments on the isolated FeMo-co, where the dominant FPPS band was at 215 cm⁻¹ [43]. A peak in this region appears in the FT spectra for all probe wavelengths, and it is particularly strong in the 560 nm data. However, the NRVS spectrum exhibits only a poorly resolved weak shoulder. As discussed in the previous paragraph, the EFF and DFT calculations find a mode in this region, which is identified as a symmetric 'breathing' mode with mostly bridging S motion. Such an assignment makes sense, because a mode with mostly S motion would be relatively weak in the NRVS. The predicted peaks at 96 and 121 cm⁻¹ can be aligned
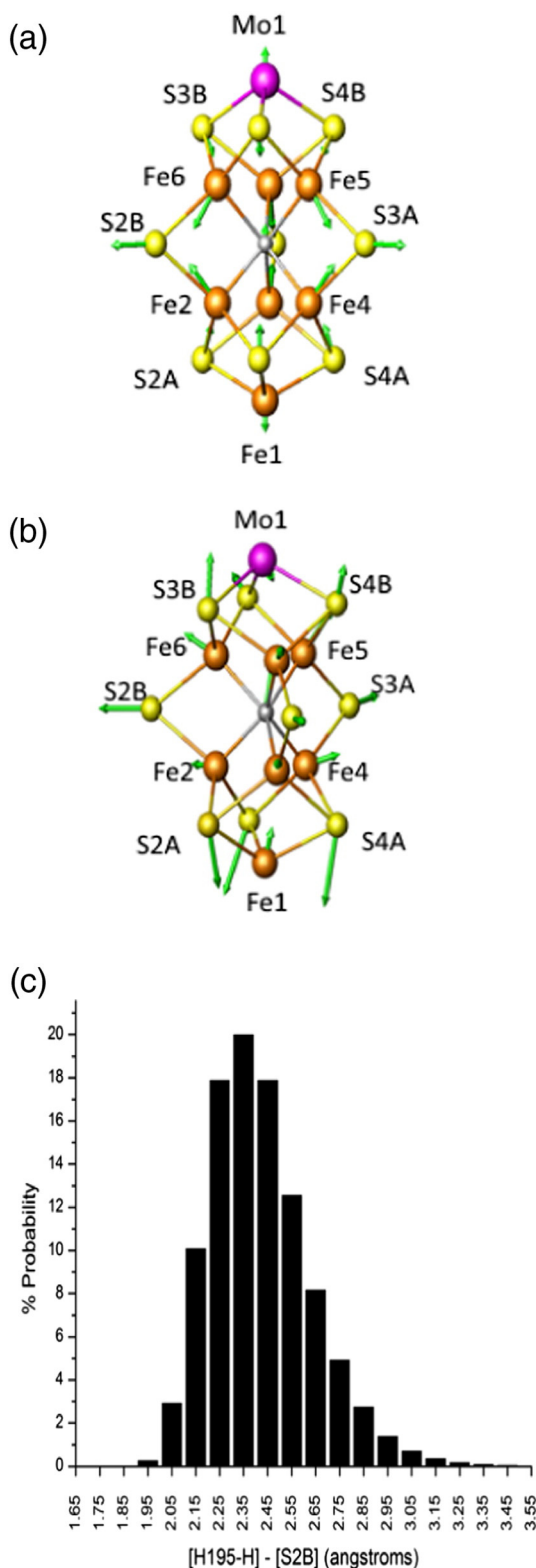
Fig. 5. Atomic motion in the FeMo-cofactor mode observed at 226 cm^{-1} by FPPS. (a) Atomic motion from EFF for the symmetric normal mode predicted at 225 cm^{-1}. (b) Atomic motion from DFT for a similar normal mode predicted at 229 cm^{-1}. (c) Histogram of the S2B–H (α-195His) distances derived from a MD simulation.

nicely with features in the FPPS data, as well as with one feature in the NRVS.

Comparisons between FPPS and RR spectra have met with success for both heme proteins [41,71,72] and for blue copper proteins [39]. In our case, the RR signal from the MoFe protein was very weak, in keeping with the reputation N$_2$ase has for being a 'black hole' for Raman spectroscopy [73]. We present the results of such measurements in part to show the difficulty of RR in this region. Despite the weak signal intensity, there are certain reproducible features with their band positions common between the RR and FPPS experiments. The strongest peak in the RR is a band due to crystalline H$_2$O/D2O ('ice') at ~213/223 cm^{-1} (Fig. 4c), which unfortunately obscures the region of most interest for comparison with the FPPS data. There is an additional ice band at ~290 cm^{-1}. Between these bands, there are weak, but reproducible, RR bands at ~240 and 261 cm^{-1} that compare favorably with a Fe–S cluster stretching mode seen in this region [57,74]. In the higher frequency region there are more intense RR bands from 338 to 382 cm^{-1} that compare favorably with FPPS and NRVS peaks in this region.

4.2. Observation of a candidate 'promoting vibration'

Apart from filling a void in our spectroscopic understanding of N$_2$ase, the FPPS spectra may help describing in the catalytic mechanism of this enzyme. The low frequency motions that we observe may be relevant to the transfer of electrons and/or protons. In the case of heme proteins, it has been often noted that lower frequency modes around and below 200 cm^{-1} are thermally populated at room temperature and are candidates for 'reactive coordinates' or 'promoting vibrations' for metalloprotein functions such as ligand binding and electron transfer [41,71]. A recent proposal suggests that coupling of heme and polypeptide vibrational motion plays a role in electron transfer [75]. The approximately symmetric breathing mode observed at ~226 cm^{-1}, with its associated cluster distortion, could be similarly relevant for electron transfer, with or without coupling to proton transfer, to the FeMo-cofactor. If the reduction of the FeMo-cofactor involves an expansion of the central cage, then the motion associated with the 226 cm^{-1} mode makes it ideal as a 'promoting vibration' for facilitating electron transfer from the P-cluster.

Promoting vibrations have also been invoked for hydrogen-transfer reactions, which often occur by tunneling as opposed to over-the-barrier mechanisms [76–78]. The proposed reaction mechanisms for N$_2$ase are replete with net H-atom transfer steps, with accumulation of 2 hydrides and 2 protons proposed for the E$_4$H$_4$ Janus intermediate [79], and an overall requirement for 8 such steps. With N$_2$ase, it is common to invoke proton transfer through either specific portions of the protein backbone or amino-acid side chains to the bridging sulfides of the FeMo-cofactor, for example, from α-195His to the waist-level bridging sulfide (S2B) [80,81] or from a water 'proton wire' to another bridging sulfide (S3B) [82]. Although this proposal is untested and speculative at the moment, it seems reasonable that certain FeMo-cofactor normal modes could act as such 'promoting vibrations' and that their possible catalytic contributions should be seriously considered.

Activation of the 226 cm^{-1} mode would enhance motion of S2B towards the H bound to α-195His, and presumably accelerate the transfer of this proton from the histidine to the sulfide. Similarly, motion of S3B would enhance proton transfer from the water chain to the FeMo-cofactor. To be modestly more quantitative about these effects, we present a brief analysis to estimate the possible significance of such motions. From the DFT normal mode analysis, we estimate that the ground state r.m.s. motion of S2B in the 226 cm^{-1} mode is ~0.16 Å. For a Boltzmann distribution at 25 °C, about 1/3 of the molecules will be in the first excited state, and about 11% in the 2nd vibrational excited state [83]. Assuming that these vibrational excited states, or "hot bands", behave as harmonic oscillators, the r.m.s. motion is enhanced by $\sqrt{3}$ and $\sqrt{5}$ vs. the ground state motion [84], thus to 0.28 and 0.36 Å, respectively. We assume an initial S2B–H distance of 2.27 Å and a favored S2B–H bond length of 1.34 Å [85]. Considering these approximations, it is possible the motion in the first and second vibrational excited states would bring the α-195His-bound proton within 0.65 or 0.57 Å, respectively, of the favored S–H bond length. Because hydrogen tunneling occurs over

this same range of distances [86], it seems reasonable that the 226 cm^{-1} mode could again qualify as a thermally activated 'promoting vibration'. Although the assignment of such a role might be thought to imply a solvent kinetic isotope effect on N$_2$ase turnover, none is observed [87–90] because substrate reduction is not rate limiting; that step belongs to the dissociation of the Fe-protein/MoFe-protein complex, which must occur for catalysis to proceed [91].

5. Conclusions

In summary, the application of FPPS to a N$_2$ase component protein has allowed us to detect a variety of low frequency normal modes that are difficult to observe by other methods. For example, the strongest modes in the FPPS are in the frequency range from 84 to 230 cm^{-1}, which is relatively difficult to reach for RR spectroscopy. The FPPS results, in association with more standard vibrational spectroscopy techniques, such as NRVS and RR, have allowed the observed vibrations to be assigned based on normal mode calculations using both EFF and DFT methods. The assigned vibrational modes have been found to have potential relevance to the catalytic activity of N$_2$ase. In particular, the 226 cm^{-1} 'breathing' mode of the FeMo-cofactor can be viewed as a potential 'promoting vibration' in the H-atom transfer (or proton-coupled electron transfer) processes that are an essential feature of N$_2$ase catalysis. Moreover, our preliminary attempt to analyze this potential role quantitatively, using the S2B-α195His interaction, adds considerable substance to this suggestion.

An additional advantage that accrues with the FPPS experiments is that they are conducted in solution at room temperature and so sample the protein in its natural environment in contrast to most other applicable spectroscopic measurements on N$_2$ase, which require cryogenic conditions. Thus, the ability to provide room-temperature information about the vibrational dynamics of the FeMo-cofactor in solution at reasonable concentrations clearly shows that FPPS is a promising technique for future investigations of reactive N$_2$ase species on catalytically relevant time scales.

Acknowledgments

References

[1] J. Olivares, E.J. Bedmar, J. Sanjuan, Mol. Plant Microbe Interact. 26 (2013) 486–494.
[2] J.N. Galloway, A.R. Townsend, J.W. Erisman, M. Bekunda, Z. Cai, J.R. Freney, L.A. Martinelli, S.P. Seitzinger, M.A. Sutton, Science 320 (2008) 889–892.
[3] D.E. Canfield, A.N. Glazer, P.G. Falkowski, Science 330 (2010) 192–196.
[4] Quantum Sphere: Applications - Ammonia Synthesis Available from: http://qsinano.com/applications/.
[5] H.-B. wikipedia Available from: http://en.wikipedia.org/wik/Haber-Bosch.
[6] J.W. Peters, R.K. Szilagyi, Curr. Opin. Chem. Biol. 10 (2006) 101–108.
[7] B.M. Barney, H.I. Lee, P.C. Dos Santos, B.M. Hoffman, D.R. Dean, L.C. Seefeldt, Dalton Trans. (2006) 2277–2284.
[8] I. Dance, Chem. Asian J. 2 (2007) 936–946.
[9] N. Schindelin, C. Kisker, J.L. Sehlessman, J.B. Howard, D.C. Rees, Nature 387 (1997) 370–376.
[10] F.A. Tezcan, J.T. Kaiser, D. Mustafi, M.Y. Walton, J.B. Howard, D.C. Rees, Science 309 (2005) 1377–1380.
[11] P.E. Bishop, R. Premakumar, D.R. Dean, M.R. Jacobson, J.R. Chisnell, T.M. Rizzo, J. Kopczynski, Science 232 (1986) 92–94.
[12] R.R. Eady, Chem. Rev. 96 (1996) 3013–3030.
[13] K.M. Lancaster, M. Roemelt, P. Ettenhuber, Y. Hu, M.W. Ribbe, F. Neese, U. Bergmann, S. DeBeer, Science 334 (2011) 974–977.
[14] T. Spatzal, M. Aksoyoglu, L. Zhang, S.L. Andrade, E. Schleicher, S. Weber, D.C. Rees, O. Einsle, Science 334 (2011) 940.
[15] P.C. Dos Santos, R.Y. Igarashi, H.-I. Lee, B.M. Hoffman, L.C. Seefeldt, D.R. Dean, Acc. Chem. Res. 38 (2005) 208–214.
[16] O. Einsle, F.A. Tezcan, S.L.A. Andrade, B. Schmid, M. Yoshida, J.B. Howard, D.C. Rees, Science 297 (2002) 1696–1700.
[17] R.Y. Igarashi, L.C. Seefeldt, Crit. Rev. Biochem. Mol. Biol. 38 (2003) 351–384.
[18] L.C. Seefeldt, B.M. Hoffman, D.R. Dean, Annu. Rev. Biochem. 78 (2009) 701–722.
[19] J. Christiansen, V.L. Cash, L.C. Seefeldt, D.R. Dean, J. Biol. Chem. 275 (2000) 11459–11464.
[20] C.C. Lee, Y. Hu, M.W. Ribbe, Science 329 (2010) 642.
[21] C.C. Lee, Y. Hu, M.W. Ribbe, Angew. Chem. 50 (2011) 5545–5547.
[22] Y. Hu, C.C. Lee, M.W. Ribbe, Science 333 (2011) 753–755.
[23] Z.Y. Yang, D.R. Dean, L.C. Seefeldt, J. Biol. Chem. 286 (2011) 19417–19421.
[24] M. Sorlie, J. Christiansen, D.R. Dean, B.J. Hales, J. Am. Chem. Soc. 121 (1999) 9457–9458.
[25] R.Y. Igarashi, M. Laryukhin, P.C. Dos Santos, H.-I. Lee, D.R. Dean, L.C. Seefeldt, B.M. Hoffman, J. Am. Chem. Soc. 127 (2005) 6231–6241.
[26] B.M. Barney, D. Lukoyanov, R.Y. Igarashi, M. Laryukhin, T.C. Yang, D.R. Dean, B.M. Hoffman, L.C. Seefeldt, Biochemistry 48 (2009) 9094–9102.
[27] B.M. Barney, D. Lukoyanov, T.C. Yang, D.R. Dean, B.M. Hoffman, L.C. Seefeldt, Proc. Natl. Acad. Sci. 103 (2006) 17113–17118.
[28] B.M. Barney, M. Laryukhin, R.Y. Igarashi, H.I. Lee, P.C. Dos Santos, T.C. Yang, B.M. Hoffman, D.R. Dean, L.C. Seefeldt, Biochemistry 44 (2005) 8030–8037.
[29] B.M. Barney, T.-C. Yang, R.Y. Igarashi, P.C.D. Santos, M. Laryukhin, H.-I. Lee, B.M. Hoffman, D.R. Dean, L.C. Seefeldt, J. Am. Chem. Soc. 127 (2005) 14960–14961.
[30] Z.-Y. Yang, L.C. Seefeldt, D.R. Dean, S.P. Cramer, S.J. George, Angew. Chem. 123 (2011) 286–289.
[31] L. Yan, C.H. Dapper, S.J. George, H.-X. Wang, D. Mitra, W.-B. Dong, W.E. Newton, S.P. Cramer, Eur. J. Inorg. Chem. 2011 (2011) 2064–2074.
[32] L. Yan, V. Pelmenschikov, C.H. Dapper, A.D. Scott, W.E. Newton, S.P. Cramer, Chem. Eur. J. 18 (2012) 16349–16357.
[33] A. Scott, V. Pelmenschikov, Y. Guo, H. Wang, L. Yan, S. George, C. Dapper, W. Newton, Y. Yoda, Y. Tanaka, S.P. Cramer, J. Am. Chem. Soc. 136 (2014) 15942–15954.
[34] V. Pelmenschikov, D.A. Case, L. Noodleman, Inorg. Chem. 47 (2008) 6162–6172.
[35] S. Nakashima, Y. Nagasawa, K. Seike, T. Okada, M. Sato, T. Kohzuma, Chem. Phys. Lett. 331 (2000) 396–402.
[36] T. Cimei, A.R. Bizzarri, S. Cannistraro, G. Cerullo, S. De Silvestri, Chem. Phys. Lett. 362 (2002) 497–503.
[37] I. Delfino, C. Manzoni, K. Sato, C. Dennison, G. Cerullo, S. Cannistraro, J. Phys. Chem. B 110 (2006) 17252–17259.
[38] Y. Nagasawa, K. Fujita, T. Katayama, Y. Ishibashi, H. Miyasaka, T. Takabe, S. Nagao, S. Hirota, Phys. Chem. Chem. Phys. 12 (2010) 6067–6075.
[39] A.R. Bizzarri, D. Brida, S. Santini, G. Cerullo, S. Cannistraro, J. Phys. Chem. B 116 (2012) 4192–4198.
[40] M.R. Armstrong, J.P. Ogilvie, M.L. Cowan, A.M. Nagy, R.J. Miller, Proc. Natl. Acad. Sci. 100 (2003) 4990–4994.
[41] V. Karunakaran, A. Benabbas, H. Youn, P.M. Champion, J. Am. Chem. Soc. 133 (2011) 18816–18827.
[42] V. Karunakaran, I. Denisov, S.G. Sligar, P.M. Champion, J. Phys. Chem. B 115 (2011) 5665–5677.
[43] I. Delfino, G. Cerullo, S. Cannistraro, C. Manzoni, D. Polli, C. Dapper, W.E. Newton, Y. Guo, S.P. Cramer, Angew. Chem. 49 (2010) 3912–3915.
[44] G.W. Strandberg, P.W. Wilson, Can. J. Microbiol. 14 (1968) 25–31.
[45] C.H. Kim, W.E. Newton, D.R. Dean, Biochemistry 34 (1995) 2798–2808.
[46] Y. Xiao, K. Fisher, M.C. Smith, W.E. Newton, D.A. Case, S.J. George, H. Wang, W. Sturhahn, E.E. Alp, J. Zhao, Y. Yoda, S.P. Cramer, J. Am. Chem. Soc. 128 (2006) 7608–7612.
[47] C. Manzoni, D. Polli, G. Cerullo, Rev. Sci. Instrum. 77 (2006) 023103.
[48] D. Polli, L. Luer, G. Cerullo, Rev. Sci. Instrum. 78 (2007) 103–108.
[49] T. Simanouti, J. Chem. Phys. 17 (1949) 245–248.
[50] E. Dowty, Phys. Chem. Miner. 14 (1987) 67–79.
[51] E. Dowty, Phys. Chem. Miner. 14 (1987) 122–138.
[52] J.P. Perdew, K. Burke, M. Ernzerhof, Phys. Rev. Lett. 77 (1996) 3865–3868.
[53] Jaguar, version 7.9 Schrödinger, LLC, New York, NY, 2012.
[54] M.J. Frisch, G.W. Trucks, H.B. Schlegel, G.E. Scuseria, M.A. Robb, J.R. Cheeseman, V.G. Zakrzewski, J.A.J. Montgomery, R.E. Stratmann, J.C. Burant, S. Dapprich, J.M. Millam, A.D. Daniels, K.N. Kudin, M.C. Strain, O. Farkas, J. Tomasi, V. Barone, M. Cossi, R. Cammi, B. Mennucci, C. Pomelli, C. Adamo, S. Clifford, J. Ochterski, G.A. Petersson, P.Y. Ayala, Q. Cui, K. Morokuma, D.K. Malick, A.D. Rabuck, K. Raghavachari, J.B. Foresman, J. Cioslowski, J.V. Ortiz, B.B. Stefanov, G. Liu, A. Liashenko, P. Piskorz, I. Komaromi, R. Gomperts, R.L. Martin, D.J. Fox, T. Keith, M.A. Al-Laham, C.Y. Peng, A. Nanayakkara, C. Gonzalez, M. Challacombe, P.M.W. Gill, B. Johnson, W. Chen, M.W. Wong, J.L. Andres, M. Head-Gordon, E.S. Replogle, J.A. Pople, Gaussian Inc., Pittsburgh, PA, 2003.
[55] D. Mitra, S.J. George, Y. Guo, S. Kamali, S. Keable, J.W. Peters, V. Pelmenschikov, D.A. Case, S.P. Cramer, J. Am. Chem. Soc. 135 (2013) 2530–2543.
[56] V. Pelmenschikov, Y. Guo, H. Wang, S.P. Cramer, D.A. Case, Faraday Discuss. 148 (2011) 409–420 (discussion 421–441).
[57] D. Mitra, V. Pelmenschikov, Y. Guo, D.A. Case, H. Wang, W. Dong, M.L. Tan, T. Ichiye, F.E. Jenney, M.W. Adams, Y. Yoda, J. Zhao, S.P. Cramer, Biochemistry 50 (2011) 5220–5235.
[58] Y. Guo, H. Wang, Y. Xiao, S. Vogt, R.K. Thauer, S. Shima, P.I. Volkers, T.B. Rauchfuss, V. Pelmenschikov, D.A. Case, E.E. Alp, W. Sturhahn, Y. Yoda, S.P. Cramer, Inorg. Chem. 47 (2008) 3969–3977.
[59] I. Dance, Inorg. Chem. 45 (2006) 5084–5091.

[60] L. Noodleman, C.Y. Peng, D.A. Case, J.M. Mouesca, Coord. Chem. Rev. 144 (1995) 199–244.
[61] T. Lovell, J. Li, T. Liu, D.A. Case, L. Noodleman, J. Am. Chem. Soc. 123 (2001) 12392–12410.
[62] P.J. Stephens, C.E. McKenna, B.E. Smith, H.T. Nguyen, M.C. McKenna, A.J. Thomson, F. Devlin, J.B. Jones, Proc. Natl. Acad. Sci. 76 (1979) 2585–2589.
[63] L.D. Book, D.C. Arnett, H.B. Hu, N.F. Scherer, J. Phys. Chem. A 102 (1998) 4350–4359.
[64] W.T. Pollard, S.L. Dexheimer, Q. Wang, L.A. Peteanu, C.V. Shank, R.A.J. Mathies, 96 (1992) 6147–6158.
[65] M.L. Tan, A.R. Bizzarri, Y. Xiao, S. Cannistraro, T. Ichiye, C. Manzoni, G. Cerullo, M.W. Adams, F.E. Jenney Jr., S.P. Cramer, J. Inorg. Biochem. 101 (2007) 375–384.
[66] L.B. Gee, I. Leontyev, A. Stuchebrukhov, A.D. Scott, V. Pelmenschikov, S.P. Cramer, Biochemistry 54 (2015) 3314–3319 (American Chemical Society).
[67] S.L. Dexheimer, Q. Wang, L.A. Peteanu, W.T. Pollard, R.A. Mathies, C.V. Shank, Chem. Phys. Lett. 188 (1992) 61–66.
[68] A.T.N. Kumar, F. Rosca, A. Widom, P.M. Champion, J. Chem. Phys. 114 (2001) 701–724.
[69] S. Ruhman, A.G. Joly, K.A. Nelson, J. Chem. Phys. 86 (1987) 6563–6565.
[70] W.T. Pollard, R.A. Mathies, Annu. Rev. Phys. Chem. 43 (1992) 497–523.
[71] F. Gruia, M. Kubo, X. Ye, P.M. Champion, Biophys. J. 94 (2008) 2252–2268.
[72] L.Y. Zhu, W. Wang, J.T. Sage, P.M. Champion, J. Raman Spectrosc. 26 (1995) 527–534.
[73] U. Bergmann, W. Sturhahn, D.E. Linn, F.E. Jenney Jr., M.W.W. Adams, K. Rupnik, B.J. Hales, E.E. Alp, A. Mayse, S.P. Cramer, J. Am. Chem. Soc. 125 (2003) 4016–4017.
[74] A. Kern, C. Näther, F. Tuczek, Inorg. Chem. 43 (2004) 5011–5020.
[75] M.G. Galinato, J.G. Kleingardner, S.E. Bowman, E.E. Alp, J. Zhao, K.L. Bren, N. Lehnert, Proc. Natl. Acad. Sci. 109 (2012) 8896–8900.
[76] S. Hay, N.S. Scrutton, Nat. Chem. 4 (2012) 161–168.
[77] C.R. Pudney, A. Guerriero, N.J. Baxter, L.O. Johannissen, J.P. Waltho, S. Hay, N.S. Scrutton, J. Am. Chem. Soc. 135 (2013) 2512–2517.
[78] S. Hay, C.R. Pudney, T.A. McGrory, J. Pang, M.J. Sutcliffe, N.S. Scrutton, Angew. Chem. 48 (2009) 1452–1454.
[79] B.M. Hoffman, D. Lukoyanov, Z.Y. Yang, D.R. Dean, L.C. Seefeldt, Chem. Rev. 114 (2014) 4041–4062.
[80] M.C. Durrant, Biochem. J. 355 (2001) 569–576.
[81] K. Fisher, N.D. Hare, W.E. Newton, Biochemistry 53 (2014) 6151–6160.
[82] I. Dance, Chem. Commun. (Camb.) 49 (2013) 10893–10907.
[83] Hyperphysics: Population Fraction Available from: http://hyperphysics.phy-astr.gsu.edu/hbase/kinetic/popfrac.html.
[84] S.J. Cyvin, Journal (1968) (Pages).
[85] Average Bond Length Differences by Model Chemistry Available from: http://cccbdb.nist.gov/bondlengthmodel2.asp?method=12&basis=6.
[86] J.P. Klinman, Biochim. Biophys. Acta 1757 (2006) 981–987.
[87] D. Mayweather, K. Danyal, D.R. Dean, L.C. Seefeldt, B.M. Hoffman, Biochemistry 51 (2012) 8391–8398.
[88] D. Lukoyanov, B.M. Barney, D.R. Dean, L.C. Seefeldt, B.M. Hoffman, Proc. Natl. Acad. Sci. 104 (2007) 1451–1455.
[89] D. Lukoyanov, Z.Y. Yang, S. Duval, K. Danyal, D.R. Dean, L.C. Seefeldt, B.M. Hoffman, Inorg. Chem. 53 (2014) 3688–3693.
[90] B.K. Burgess, S. Wherland, W.E. Newton, E.I. Stiefel, Biochemistry 20 (1981) 5140–5146.
[91] R.N. Thorneley, D.J. Lowe, Biochem. J. 215 (1983) 393–403.